

## Parabolic-symmetry vector optical fields and their tightly focusing properties

Yue Pan (潘岳),<sup>1</sup> Yongnan Li (李勇男),<sup>1</sup> Zhi-Cheng Ren (任志成),<sup>1</sup> Yu Si (司宇),<sup>1</sup> Chenghou Tu (涂成厚),<sup>1</sup> and Hui-Tian Wang (王慧田)<sup>1,2,\*</sup>

<sup>1</sup>*School of Physics and MOE Key Laboratory of Weak Light Nonlinear Photonics, Nankai University, Tianjin 300071, China*

<sup>2</sup>*National Laboratory of Solid State Microstructures, Nanjing University, Nanjing 210093, China*

(Received 20 November 2013; published 10 March 2014)

We present theoretically and generate experimentally a vector optical field with parabolic symmetry of linear polarization. We extend the study to the modified parabolic-symmetry vector fields. We explore their tightly focusing behaviors, in particular, a modified parabolic-symmetry vector field can be tightly focused into a high-performance subwavelength sharp line.

DOI: [10.1103/PhysRevA.89.035801](https://doi.org/10.1103/PhysRevA.89.035801)

PACS number(s): 42.25.Ja, 42.40.Jv, 42.25.Hz

Polarization is one of the most salient features of light, even more important than its coherence property. Polarization, as a degree of controlling freedom, is certainly of great importance for engineering the optical field and controlling the interaction of light with matter. Vector optical fields have attracted extensive interest due to many unique features with respect to the scalar fields, such as the far-field focal spot beyond the diffraction limit [1–4], the light needle of a longitudinally polarized field [5], the optical cage [6,7], and the optical chain [8]. In particular, the vector fields have many important applications, such as particle acceleration [9], single molecule imaging [10], near-field optics [11], nonlinear optics [12], and optical trapping and manipulation of particles [13,14].

Most previous reports focused mainly on cylindrical-symmetry vector fields [1–13,15–20]. An elliptical-symmetry vector field has also been investigated [21], for which the local linear polarizations are always along the tangential direction of concentric ellipses. Very recently, we reported other two kinds of vector fields: with linear polarization distributions modeling to field lines [22] and with bipolar symmetry of linear polarization [23].

Here we present and generate vector fields with a parabolic symmetry rather than the cylindrical, elliptical, or bipolar symmetries for spatial distribution of linear polarization. The geometric configurations of linear polarizations as an additional degree of freedom assists in controlling the field symmetry and distribution at the focus. In particular, a modified parabolic-symmetry vector field can be tightly focused into a sharp line with a dimension of  $0.57\lambda \times 1.56\lambda$  (full width at half-maximum, FWHM), which has a figure of merit being 0.65.

To generate the parabolic-symmetry vector fields, a flexible configuration with the aid of a  $4f$  system [18] is still practicable. The schematic shown in Fig. 1 is very similar to those used in Refs. [14,18,19,23]. This approach includes four key steps: (i) an input linearly polarized laser field is divided into two equiamplitude parts, which are easily achieved by use of a sine-cosine grating displayed on a spatial light modulator (SLM) in the input plane of the  $4f$  system; (ii) the two parts must carry the space-variant phase  $\delta(x,y)$ ; (iii) the two parts must pass through different optical paths, making the two

parts become orthogonally right- and left-handed circularly polarized by a pair of  $1/4$ -wave plates behind a spatial filter (SF) in the Fourier plane of the  $4f$  system; and (iv) the two parts are combined by the Ronchi phase grating (G) in the output plane of the  $4f$  system. Thus the generated vector fields can be represented as follows [18,19,23]:

$$\mathbf{E}(x,y) = A_0[\cos \delta(x,y)\hat{\mathbf{e}}_x + \sin \delta(x,y)\hat{\mathbf{e}}_y], \quad (1)$$

where  $\hat{\mathbf{e}}_x$  and  $\hat{\mathbf{e}}_y$  are the unit vectors in the  $x$  and  $y$  directions,  $A_0$  is the space-invariant amplitude, and  $\delta(x,y)$  is the two-dimensional (2D) space-variant phase carried by the grating displayed on a SLM. The vector field described by Eq. (1) is locally linearly polarized because its two orthogonal components are always in phase.

To generate the parabolic-symmetry local linearly polarized vector fields, we should first give a brief introduction to the parabolic coordinate system  $(u,v)$ , as shown in Fig. 2. This coordinate system has many applications, such as for treating the Stark effect and the potential theory of the edges. The parabolic coordinates  $(u,v)$  are defined by the Cartesian coordinates  $(x,y)$  as follows:

$$x = uv, \quad y = (v^2 - u^2)/2. \quad (2)$$

The above expressions can be rewritten as

$$2y = x^2/u^2 - u^2, \quad 2y = v^2 - x^2/v^2. \quad (3)$$

The parabolic coordinate system is also a 2D orthogonal coordinate system in which the constant- $u$  curves form a set of confocal parabolas that open upwards, whereas the constant- $v$  curves form another set of confocal parabolas that open downwards. The common focus of the two sets of parabolas is located at the origin O.

To generate the parabolic-symmetry vector fields, we should give explicit expressions of  $u$  and  $v$  as

$$u^2 = \sqrt{x^2 + y^2} - y, \quad v^2 = \sqrt{x^2 + y^2} + y. \quad (4)$$

Similarly to the generation of the cylindrical vector fields [14,18,19], in particular, of the bipolar vector fields [23], we set the space-variant phase  $\delta$  as

$$\begin{aligned} \delta &= m\pi u + n\pi v \\ &= m\pi\sqrt{\sqrt{x^2 + y^2} - y} + n\pi\sqrt{\sqrt{x^2 + y^2} + y}, \end{aligned} \quad (5)$$

\*htwang@nankai.edu.cn; htwang@nju.edu.cn

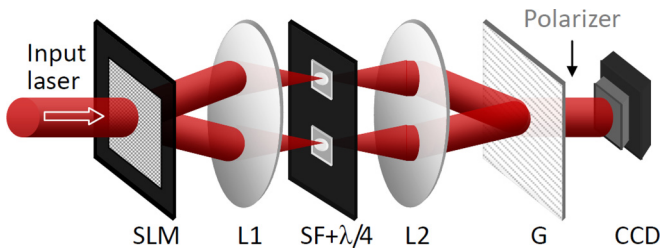


FIG. 1. (Color online) Schematic for generating the vector fields. A SLM is located at the input plane of the  $4f$  system composed of a pair of lenses (L1 and L2). Two  $1/4$ -wave plates behind a SF are placed in the Fourier plane of the  $4f$  system. A Ronchi grating (G) is placed in the output plane of the  $4f$  system. A linear polarizer may be inserted between G and CCD to acquire the intensity patterns by CCD.

where the signs of  $u$  and  $v$  are included into  $m$  and  $n$ , because  $m$  and  $n$  can be positive or negative.  $m$  and  $n$  are the *topological charges* in the  $u$  and  $v$  dimensions in the parabolic coordinate system, respectively. The polarization distribution of the vector field when  $\delta$  has the form in Eq. (5) exhibits a parabolic symmetry.

We now will explore the situations when  $\delta$  depends only on  $u$  ( $m \neq 0$  and  $n \equiv 0$ ). As shown in Fig. 3, the generated parabolic-symmetry vector fields have no polarization singularity, which are similar to the vector fields with the radially variant polarization distributions [15] but which differ from the cylindrical vector fields with one singularity [1–13,15–20], elliptical-symmetry vector fields with one singularity [21], bipolar vector fields with two singularities [23], and field-line-like vector fields with two or more singularities [22]. Total intensity pattern exhibits the uniform distribution. The simulated results are in good agreement with the measured ones for the  $x$ -component intensity patterns, which are

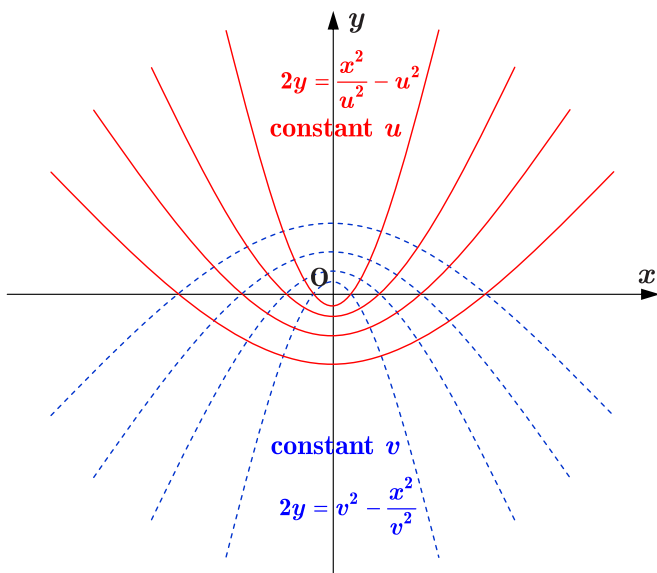


FIG. 2. (Color online) Parabolic coordinate system  $(u, v)$ . A set of solid (dashed) curves show the constant- $u$  ( $-v$ ) parabolas. All these parabolic curves have the same focus located at the origin O.  $(x, y)$  is the Cartesian coordinate system.

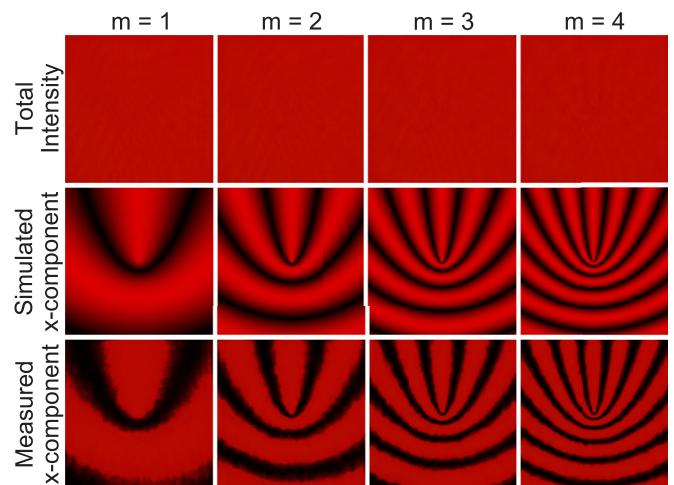


FIG. 3. (Color online) Generated parabolic-symmetry vector fields with the polarization distribution dependent only on  $u$  for different  $m$  when  $n \equiv 0$ .

composed of a set of open-upward parabolas. The extinction or light-passing parabolas have a common focus and their amount increases as  $m$  increases. The polarization distributions of the generated vector fields indeed depend only on  $u$  (the locations with the same polarization form a constant- $u$  parabola). We should emphasize that we will not show the total intensity patterns of all the generated parabolic-symmetry vector fields below, because they are the same as those shown in the first row of Fig. 3.

Figure 4 shows the generated vector fields with the polarization distributions dependent only on  $v$  ( $m \equiv 0$  and  $n \neq 0$ ) for different  $n$ . As shown in the first and second rows, the measured  $x$ -component patterns are in good agreement with the simulated results. Any pattern is composed of a set of open-downward parabolas, implying that the polarization distributions depend only on  $v$  (locations with the same polarization lie in a constant- $v$  open-downward parabola). The  $x$ -component patterns for  $m \equiv 0$  and  $n \neq 0$  exhibit the mirror symmetry about the  $y$  axis, like the cases for  $m \neq 0$  and  $n \equiv 0$  in Fig. 3.

We now explore the cases when  $\delta$  depends on both  $u$  and  $v$  ( $m \neq 0$  and  $n \neq 0$ ). Figure 5 shows the generated vector fields with the polarization distributions dependent on both  $u$  and  $v$

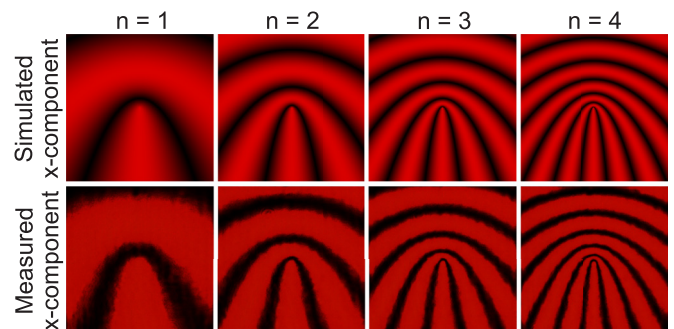


FIG. 4. (Color online) Generated parabolic-symmetry vector fields with the polarization distribution dependent only on  $v$  for different  $n$  when  $m \equiv 0$ .

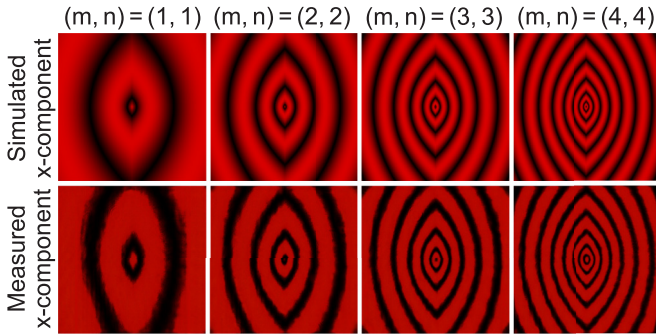


FIG. 5. (Color online) Generated parabolic-symmetry vector fields with the polarization distribution dependent on both  $u$  and  $v$  for different combination of  $m$  and  $n$  when  $m = n$ .

when  $m = n$ . The  $x$ -component intensity patterns exhibit an eyelidlike shape. The amount of “eyelid” equals to  $2m$  (or  $2n$ ).

Figure 6 shows another kind of vector fields when  $\delta$  is dependent on both  $u$  and  $v$  for  $m \equiv 4$ . When  $n$  is changed from 0 to 4, the  $x$ -component intensity patterns change from the open-upward parabolas to an eyelidlike shape. In particular, the symmetry changes from the mirror symmetry about the  $y$  axis only to the higher symmetry (the mirror symmetry about both the  $x$  and  $y$  axes). In the two cases of  $(m, n) = (4, 1)$  and  $(4, 2)$ , the  $x$ -component patterns look like the flame of the candle.

Below we will explore a kind of modified parabolic-symmetry vector fields, where the space-variant phase  $\delta$  is taken as a quadratic function of  $u$  and  $v$  as follows:

$$\delta = m\pi u^2 + n\pi v^2. \quad (6)$$

With Eq. (4), the above expression can be rewritten as

$$\begin{aligned} \delta &= (m+n)\pi\sqrt{x^2+y^2} - (m-n)\pi y \\ &= p\pi\sqrt{x^2+y^2} - q\pi y, \end{aligned} \quad (7)$$

where we have defined two new “topological charges” as  $p = m+n$  and  $q = m-n$ . Figure 7 shows the generated vector fields for different  $p$  ( $=0, 1, 2, 3, 4$ ) when  $q \equiv 4$ . As shown in the first column of Fig. 7, when  $p = 0$  the polarization distribution is a function of  $y$  only, because  $\delta$  in Eq. (7) depends only on  $y$  when  $p = 0$  and  $q \neq 0$ . As  $p$  increases when  $q \equiv 4$ , as shown from the second column to the fifth column in Fig. 7, the patterns of the trajectories with same polarization are very similar to a phenomenon that when a small rounded triangle is

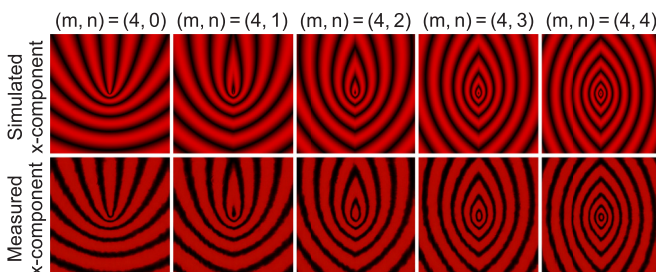


FIG. 6. (Color online) Generated parabolic-symmetry vector fields with the polarization distribution dependent on both  $u$  and  $v$  for different  $n$  when  $m \equiv 4$ .

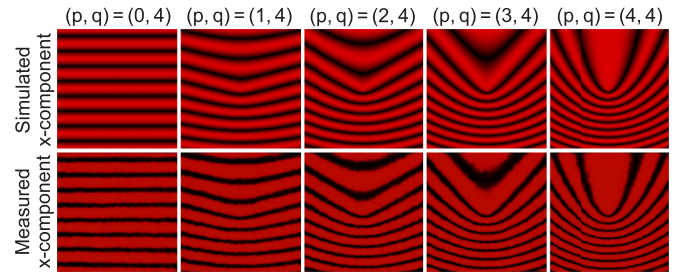


FIG. 7. (Color online) Modified parabolic-symmetry vector fields for different  $p$  when  $q \equiv 4$ .

placed on the layered plasticine, the deformation of the layered plasticine becomes large as the pressure increases.

Figure 8 shows the generated vector fields for different  $q$  ( $=0, 1, 2, 3, 4$ ) when  $p \equiv 4$ . When  $q = 0$ , as shown in the first column, the  $x$ -component intensity pattern exhibits a concentric annulus structure, which indicates the polarization to be radially variant only, because  $\delta$  in Eq. (7) is a function of radial coordinate  $r = \sqrt{x^2 + y^2}$  only when  $p \neq 0$  and  $q = 0$ . As  $q$  increases, as shown from the second column to the fifth column in Fig. 8, the  $x$ -component intensity patterns exhibit a series of ellipses with one same focus as the origin (when  $p \neq q$ ) to a series of confocal parabolas (when  $p = q$ ). When  $(p, q) = (4, 3)$ , the pattern is similar to the peacock’s fine tail feather.

In the above, we focus on the generation of various parabolic-symmetry vector fields. It is very interesting to explore the tight focusing behaviors of this kind of vector fields. The so-called tight focusing is that a lens with a high numerical aperture (NA) is used, which is usually 0.8 or larger [1,2,24]. As mentioned above, the polarization distributions of the parabolic-symmetry vector fields are neither vertically nor horizontally symmetric (despite that the intensity patterns exhibit the vertical and/or horizontal symmetry), which result in the tight focusing patterns lacking the vertical and/or horizontal symmetry. We now will explore the tight focusing behavior of a modified parabolic-symmetry vector field with the sign of its  $x$  component in the  $x < 0$  region being changed. Referencing Eq. (1), this modified vector field with  $\delta$  obeying Eq. (5) can be written as

$$\mathbf{E}(x, y) = A_0[\text{sgn}(x) \cos \delta(x, y)\hat{\mathbf{e}}_x + \sin \delta(x, y)\hat{\mathbf{e}}_y], \quad (8)$$

where  $\text{sgn}(x)$  is the well-known sign function. By the Richards-Wolf integrals [24,25], we simulate the tightly focused field of

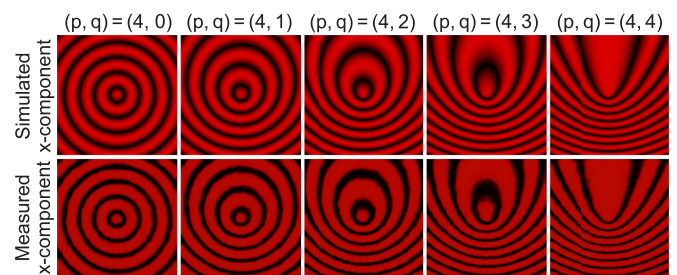


FIG. 8. (Color online) Modified parabolic-symmetry vector fields for different  $q$  when  $p \equiv 4$ .

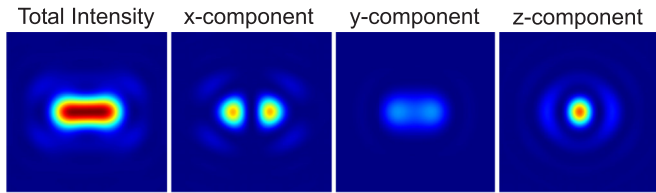


FIG. 9. (Color online) Simulated tightly focused field for the modified parabolic-symmetry vector field with  $(m,n) = (0.45,0.8)$  by use of a lens with  $NA = 0.9$ . Any picture has a dimension of  $4\lambda \times 4\lambda$ .

the modified parabolic-symmetry vector field with  $(m,n) = (0.45,0.8)$  by a lens with  $NA = 0.9$ , as shown in Fig. 9. Total intensity pattern exhibits a flattop sharp line with a subwavelength size of  $\sim 0.57\lambda$  in the  $y$  direction and a size of  $\sim 1.56\lambda$  in the  $x$  direction, which is larger than the reported sharp lines [23,24]. We appraise its figure of merit (which is defined as the full width at 95% of the maximum divided by FWHM) to be 0.65 being superior to 0.56 in Refs. [23,24].

At last, we emphasize that all the generated parabolic-symmetry vector fields have the same dimensions of  $\sim 5 \times 5 \text{ mm}^2$  and the uniform intensity distribution. The parabolic-symmetry vector fields are not the eigensolutions of the paraxial wave equation. However, these vector fields can be decomposed into a series of eigenmodes. As the well-known limited plane wave, it is also not the eigensolution of the

paraxial wave equation but is also the superposition of a series of eigenmodes. We conformed experimentally that the generated vector field could propagate steadily because when it is imaged by a lens, the imaged one holds all the properties of the original vector field.

In summary, we designed theoretically and generated experimentally a kind of local linearly polarized vector fields with the parabolic symmetry of linear polarization, which breaks the cylindrical, elliptical, and bipolar symmetry. In addition, we also extended our study to the modified parabolic-symmetry vector fields. The engineerable geometric configuration of polarization provides a powerful way in controlling the tight focusing field at the focus to some specific applications. We should also point out that this kind of vector field has no polarization singularity. In particular, by designing the polarization configuration of a modified parabolic-symmetry vector field, under the tight focusing condition, a high-performance subwavelength sharp line could be achieved, which has a figure of merit as high as 0.65 and the important applications such as lithography and optical storage.

This work was supported by the National Basic Research Program of China under Grant No. 2012CB921900, the National Natural Science Foundation of China under Grants No. 11374166 and No. 10934003, and the National Scientific Instrument and Equipment Development Project under Grant No. 2012YQ17004.

- 
- [1] Q. Zhan, *Adv. Opt. Photon.* **1**, 1 (2009).  
 [2] K. S. Youngworth and T. G. Brown, *Opt. Express* **7**, 77 (2000).  
 [3] R. Dorn, S. Quabis, and G. Leuchs, *Phys. Rev. Lett.* **91**, 233901 (2003).  
 [4] X. Hao, C. Kuang, T. Wang, and X. Liu, *Opt. Lett.* **35**, 3928 (2010).  
 [5] H. Wang, L. Shi, B. Lukyanchuk, C. Sheppard, and C. T. Chong, *Nat. Photon.* **2**, 501 (2008).  
 [6] Y. Kozawa and S. Sato, *Opt. Lett.* **31**, 820 (2006).  
 [7] X. L. Wang, J. Ding, J. Q. Qin, J. Chen, Y. X. Fan, and H. T. Wang, *Opt. Commun.* **282**, 3421 (2009).  
 [8] Y. Q. Zhao, Q. Zhan, Y. L. Zhang, and Y. P. Li, *Opt. Lett.* **30**, 848 (2005).  
 [9] C. Varin and M. Piche, *Appl. Phys. B* **74**, s83 (2002).  
 [10] L. Novotny, M. R. Beversluis, K. S. Youngworth, and T. G. Brown, *Phys. Rev. Lett.* **86**, 5251 (2001).  
 [11] A. Ciattoni, B. Crosignani, P. Di Porto, and A. Yariv, *Phys. Rev. Lett.* **94**, 073902 (2005).  
 [12] A. Bouhelier, M. Beversluis, A. Hartschuh, and L. Novotny, *Phys. Rev. Lett.* **90**, 013903 (2003).  
 [13] Q. W. Zhan, *Opt. Express* **12**, 3377 (2004).  
 [14] X. L. Wang, J. Chen, Y. N. Li, J. P. Ding, C. S. Guo, and H. T. Wang, *Phys. Rev. Lett.* **105**, 253602 (2010).  
 [15] J. Arlt and M. J. Padgett, *Opt. Lett.* **25**, 191 (2000).  
 [16] Z. Bomzon, G. Biener, V. Kleiner, and E. Hasman, *Opt. Lett.* **27**, 285 (2002).  
 [17] C. Maurer, A. Jesacher, S. Fürhapter, S. Bernet, and M. Ritsch-Marte, *New J. Phys.* **9**, 78 (2007).  
 [18] X. L. Wang, J. P. Ding, W. J. Ni, C. S. Guo, and H. T. Wang, *Opt. Lett.* **32**, 3549 (2007).  
 [19] X. L. Wang, Y. N. Li, J. Chen, C. S. Guo, J. P. Ding, and H. T. Wang, *Opt. Express* **18**, 10786 (2010).  
 [20] S. Liu, P. Li, T. Peng, and J. L. Zhao, *Opt. Express* **20**, 21715 (2012).  
 [21] G. Lerman, Y. Lilach, and U. Levy, *Opt. Lett.* **34**, 1669 (2009).  
 [22] Y. Pan, S. M. Li, L. Mao, L. J. Kong, Y. N. Li, C. H. Tu, P. Wang, and H. T. Wang, *Opt. Express* **21**, 16200 (2013).  
 [23] Y. Pan, Y. N. Li, S. M. Li, Z. C. Ren, Y. Si, C. H. Tu, and H. T. Wang, *Opt. Lett.* **38**, 3700 (2013).  
 [24] G. M. Lerman and U. Levy, *Opt. Lett.* **32**, 2194 (2007).  
 [25] B. Richards and E. Wolf, *Proc. Roy. Soc. A* **253**, 358 (1959).